The MUV-Visible Spectrum of H_2 Excited by Electron Impact

Geoffrey K. James, Joseph M. Ajello and Wayne R. Pryor[†]

Jet Propulsion Laboratory, California Institute of Technology, 4800 Oak Grove Drive, Pasadena CA91109

'Laboratory for Atmospheric and Space Physics, 1234 Innovation Drive, University of Colorado, Boulder, CO 80303

Abstract

The electron-impact-induced emission spectrum of H_2 has been measured in the extended wavelength region 175-530 nm at a spectral resolution of 1.7 nm (FWHM). The laboratory spectra observed in the middle ultraviolet (MUV) and visible spectral region are characterized by underlying H_2 ($a\ ^3\Sigma_g^+ \rightarrow b\ ^3\Sigma_u^+$) continuum emission, together with many strong lines assigned to the radiative decay of the *gerade* singlet states of H_2, and to members of the H Balmer series resulting from dissociative excitation of H_2. Our calibrated MUV spectral data, obtained at 14, 19 and 100 eV electron-impact energies, provide absolute emission cross sections of these H_2 lines and will assist in the interpretation of planned Galileo Ultraviolet Spectrometer observations of Jupiter's aurora in this wavelength region.

Introduction

In a companion paper (Pryor *et al.* (1998)) Galileo Ultraviolet Spectrometer (UVS) observations of Jupiter's night-side auroral spectrum in the wavelength range 160-320 nm are compared to laboratory measurements of H_2 spectra produced by electron impact excitation at 14, 19 and 100 eV. The laboratory spectra in this wavelength region are attributed to H_2 ($a\ ^3\Sigma_g^+ \rightarrow b\ ^3\Sigma_u^+$) continuum emission. The close resemblance of the UVS observations to the laboratory H_2 spectra provided evidence for the first spectral observation of H_2 (a-b) continuum emission in any astrophysical object. In anticipation of planned Galileo UVS observations of Jupiter's aurora at longer wavelengths, these laboratory measurements of electron-impact-induced emission spectra of H_2 have been extended in the present work to cover the middle ultraviolet (MUV) through visible spectral region from 175-530 run. The laboratory spectra measured in this wavelength range are characterized by the underlying H_2 ($a \rightarrow b$) continuum emission, together with many strong lines assigned to the *gerade* singlet states of H_2 (decaying to the $B\ ^1\Sigma_u^+$ state), and to members of the H Balmer series resulting from dissociative excitation of H_2.

The *gerade* singlet states of H_2 are optically forbidden from the ground state ($X\ ^1\Sigma_g^+$) and have been the subject of extensive theoretical and experimental investigations. Perhaps the most comprehensive experimental measurements of high-resolution emission spectra in hydrogen discharges were performed by Dieke (1958) and later recompiled by Crosswhite (1972). The rovibronic spectra were highly complex, due in part to mixing among the upper *gerade* manifolds. Watson and Anderson (1977) measured optical excitation functions produced by electron impact excitation of several rovibronic levels of the EF and $H\ ^1\Sigma_g^+$ states of H_2 (which decay to the $B\ ^1\Sigma_u^+$ state), together with absolute emission cross sections at 200 eV impact energy. In another electron impact study Anderson et *al. (1977)* measured the optical excitation function of the GK $^1\Sigma_g^+$ - $B\ ^1\Sigma_u^+$ (0,0) P 1,R2,R3 rovibronic line blend at 463.4 nm and determined the absolute emission cross section at 200 eV, together with the radiative lifetime of the GK ($v'=0$) state. Day *et al. (1979)* also studied electron excitation of the singlet-g states of H_2, measuring optical excitation functions, emission cross sections at 50 eV, and radiative lifetimes. Tsukiyama *et al. (1992)* investigated rovibronic levels of the singlet-g states using extreme ultraviolet-visible double-resonance spectroscopy to measure rovibronic fluorescence lifetimes and determine term values. Lifetimes of the EF, GK and $H\ ^1\Sigma_g^+$ states showed significant rotational dependence caused by nonadiabatic coupling among the upper *gerade* manifolds.

Two principal theoretical approaches have been used to calculate nonadiabatic corrections to the excited *gerade* singlet states of H_2. Ross and Jungen (1994a,b,c) used molecular multichannel quantum-defect theory, whereas Wolniewicz, Dressier and co-workers (e.g. Senn and Dressier (1987), Yu and Dressler (1994), Wolniewicz and Dressier (1994,1977)) carried out *ab initio* calculations of the nonadiabatic coupling among the upper *gerade* manifolds (EF, GK, $H\ ^1\Sigma_g^+$, $I\ ^1\Pi_g$ and $J\ ^1\Delta_g$) and evaluated term energies use the coupled-equations approach. Both methods show that the EF, GK and H states are significantly perturbed by nonadiabatic interactions and therefore their energy level patterns cannot be represented as simple power series in quantum numbers. Indeed, the Born-Oppenheimer approximation breaks down at n=2 in hydrogen. Adiabatic and nonadiabatic shifts of the rovibronic levels amount to hundreds of cm-l .

The GK and H levels are involved in a host of avoided crossings with levels of each other, with high lying levels of the EF states, and with the 1 and J states. The EF, GK and H Born-Oppenheimer states all have a rovibronic structure characterized by a double-minimum potential curve (Ross and Jungen (1994a), Yu and Dressier (1994)).

Experimental Technique

The experimental apparatus, calibration procedure, and cross section measurement technique have been described in detail in earlier publications (James *et al.* (1992), Ajello *et al.* (1989)). In brief, the apparatus used in the present measurements consists of an electron impact collision chamber in tandem with a medium resolution 1-meter UV-visible spectrometer. The MUV-visible spectrum of H_2 was measured by crossing a magnetically collimated beam of electrons at 14, 19 and 100 eV with a beam of H_2 gas formed by a capillary array. Emitted photons, corresponding to radiative decay of collisionally excited states of H_2, were detected at 90° by the UV-visible spectrometer equipped with suitable photomultiplier detectors in the wavelength range 175-530 nm. For the wavelength range 220-530 nm the detector is an EMR photoelectric trialkali E photomultiplier tube with an exceptionally low dark count rate of 2 Hz at room temperature. At lower wavelengths (175-220 nm) an EMR 542 F photomultiplier tube is used. The two spectral data sets are conveniently merged around 220nm, based on the smooth shape of the H_2 ($a \rightarrow b$) continuum emission spectrum in that region.

The measured MUV-visible H_2 emission spectra are calibrated in two stages: (1) the relative spectral sensitivity of the optical system and detector with wavelength is established, and (2) the relative spectral data are then rendered absolute by normalization to the intensity of H Balmer-β (486.1 nm) produced by dissociative excitation of H_2. The relative spectral sensitivity was calibrated using the procedure described by Ajello *et al. (1988)* for the wavelength range 175-210 nm, and by the use of NIST-calibrated deuterium and tungsten-halogen blackbody standard lamp sources of spectral irradiance for the ranges 200-350 run and 290-500 nm, respectively. The standard lamps were used to illuminate a calibrated diffuser that was masked to illuminate the same portion of the diffraction grating used in the spectral measurements with the electron beam. The relative inverse spectral sensitivity of the spectrometer and E-photomultiplier system is shown in Figure 1 over the wavelength range 220 to 500 nm, together with associated error bars. Sensitivity in the range 500-530 nm is estimated by extrapolating a fit to the measured calibration data points.

The value for the H Balmer-β (486.1 nm) cross section at 100 eV electron impact energy used to normalize the relative spectral data is from Karol is and Harting's (1978) excitation function data which was normalized at 500 eV to the cross section measured by Vroom and deHeer (1969). It was assumed that the molecular contribution in the present data was insignificant compared to the dissociative excitation component. The assumption that the molecular contribution to the observed 100 eV (486.1 nm) peak is small compared to the H Balmer-β contribution means that the reported emission cross sections represent a lower limit to the true cross sections.

The 19 eV spectrum was again normalized using the H Balmer-β feature. In this case we measured the relative intensity of H Balmer-β at 100 eV and 19 eV to be 2.75. The excitation function of Karol is and Harting (1978) was not used to derive the 19 eV cross sections since the former measurements were made at much higher spectral resolution (FWHM 0.1 nm) where the molecular contribution to the observed line intensity at 19 eV is much lower than in the present low resolution data.

Results and Discussion

Figures 2a,b,c show the calibrated MUV-visible emission spectra of H_2 within the wavelength range 175-530 run produced by electron impact at 14, 19, and 100 eV, respectively, measured at a spectral resolution of 1.7 nm (FWHM). The spectra were obtained at a gas temperature of 300 "K and with an electron beam current of approximately 100 μA. Since the observed MUV-visible lines correspond either to the decay of excited *gerade* molecular states to the B $^1\Sigma_u^+$ state or to members of the H-Balmer series (and do not couple directly with the X $^1\Sigma_g^+$ ground state) there is no possibility of self absorption due to resonance trapping, enabling the experiment to be performed at a relatively high gas pressure of 2.4x104 torr.

The H_2 MUV-visible molecular emission spectrum measured in the present experiment is characterized by an extremely open rotational structure (Watson and Anderson (1977)) with large spacing between the individual rotational lines in a given vibrational band. This results in a blending of lines corresponding to different bands within a given observed spectral feature, especially at the low spectral resolution used to ensure sufficient signal strengths in the present measurements. In general, the observed spectral features represent blends of more than one rotational line belonging to a given vibrational transition, as well as overlapping rotational lines of other vibrational band systems.

Table 1 lists the feature numbers, peak wavelengths, integrated wavelength intervals and measured emission cross sections of the observed H_2 lines at 19 and 100 eV. Also listed in the Table are spectroscopic assignments taken from the extensive compilation of Crosswhite (1 972), based on the spectroscopic data of Dieke (1958). Herzberg notation is used except where indicated in Italics that denote Crosswhite's notation. Each line is assigned to many unresolved spectroscopic components and the stated emission cross section for each feature includes the contributions from all unresolved components, as well as the underlying H_2 (a-b) continuum emission. It should be noted that due to the significant mixing of some levels the vibronic labels are sometimes of only notional convenience (Ross and Jungen (1994c)). Given that the present data are measured at low spectral resolution (FWHM 1.7 rim), and the thousands of rovibronic lines documented by Crosswhite (1972), assignments are based on those transitions that fall within ±0.3 nm of the present observed peak wavelength. The strongest transitions observed in the discharge measurements of Dieke (1958) may not necessarily correspond to the strongest transitions observed in the present single scattering experiment, but serve as an indication.

The emission cross sections reported at 19 eV and 100 eV were measured at 90° to the electron beam axis but have not been corrected for polarization. However, since the polarization

is likely to be less than 10°/0 (Watson and Anderson (1977)) this corresponds to a maximum error of approximately 3°/0 (from the (1-P/3) correction factor).

The uncertainty in the absolute emission cross sections measured in this work is estimated from the square root of the sum of the squares of the following contributing errors: (1) 7% uncertainty in the relative inverse spectral sensitivity calibration using the N] ST-calibrated lamps, (2) 12% uncertainty in the H Balmer-β cross section value of Karolis and Harting (1978) used to normalize the present data, (3) up to 3°/0 error due to the lack of a polarization correction to the present data, and (4) up to 6% uncertainty due to signal statistics and drifting of experimental parameters such as gas pressure and electron beam current. This calculation yields an overall error of approximately 160A.

No discrete features are observed at 14 eV electron impact energy and the measured emission spectrum at this energy (Figure 2a) can be attributed to the H_2 ($a\ ^3\Sigma_g^+ \rightarrow b\ ^3\Sigma_u^+$) continuum. This spin forbidden excitation of the $a\ ^3\Sigma_g^+$ state is a major dissociative channel of H_2 at low energy, with a peak cross section at 15.5 eV and a full width at half-maximum (F WHM) of the excitation function of only 7 eV (Ajello and Shemansky (1993)). The apparent rise in measured spectral intensity at wavelengths above 480 nm may be attributed to a combination of: (1) radiation also being detected in second order, (2) errors in the relative spectral calibration (which increase at the highest wavelengths), and (3) possible visible light leakage from the electron gun filament.

The high energy dependence of the H_2 ($a\ ^3\Sigma_g^+ \rightarrow b\ ^3\Sigma_u^+$) continuum cross section has a rapid $1/E^3$ fall off with electron energy, E, above 50 eV (Ajello and Shemansky (1993). This can be seen in the 100 eV spectrum (Figure 2c) which is dominated by the strong H Balmer-β and Balmer-γ lines (features 26 and 18, respectively). Balmer series members up to n=8 can be identified in the 10OeV spectrum. Transitions to the $B\ ^1\Sigma_u^+$ state from levels of the $GK\ ^1\Sigma_g^+$ state with v'=0,1,2,3, and from levels of the $H\ ^1\Sigma_g^+$ state with v'=0,1,2 have been observed at both 100 eV and 19 eV electron impact energies.

Weak H-B (2,0) P4, P6 and (2,1) P2, P4, P5 features observed by Watson and Anderson (1 977) at 370.2 and 388.9 nm, respectively, cannot be resolved in the present measurements. This is hardly surprising considering the pressure used in the present work is a factor of 100 lower.

The emission cross section measurement by Anderson *et al.* (1977) of the (blended) GK-B (0,0) P1, R2, R3 transitions at 463.4 nm yielded a total value of (1 .2±0.3) $x10^{-20}$ cm' at 200 eV. The present value of (2.66±0.42) xl 0^{-20} cm^2 measured for the equivalent (blended) feature number 22 at 100 eV, combined with the $E^{-0.83}$ energy dependence of the excitation function measured by Anderson et *al. (1977)* for this transition above 100 eV, yields an emission cross section of (1.50 ±0.24) **x10-20 cm^2** at 200 eV, based on the present datum at 100 eV. These two measurements cannot, however, be compared directly since the degree of spectral resolution used to isolate the GK-B (0,0) transition (and the integrated wavelength interval) are significantly different. Similarly, the 50 eV emission cross sections measured at 0.1 nm resolution (FWHM) by Day *et al.* (1979) in the wavelength range 386-522 nm are not directly comparable with the present measurements.

Acknowledgments

This work was carried out at the Jet Propulsion Laboratory, California Institute of Technology, and was supported by NASA Planetary Atmospheres and Astrophysics Program Offices, the Air Force Office of Scientific Research, and the Aeronomy Program of the National Science Foundation under a contract with the National Aeronautics and Space Administration. The authors thank Stephen Ross of the University of New Brunswick for helpful discussions and a critical reading of the manuscript.

Table Caption

Table 1. Emission cross sections of H_2 in the MUV-visible spectral region at 19 and 100 eV electron impact energies. Spectroscopic assignments are taken from the extensive compilation of Crosswhite (1972), using Herzberg notation except where indicated in Italics that denote Crosswhite's notation. Errors in the measured emission cross sections are estimatedtobe*16%.

Figure Captions

Figure 1. The MUV-visible calibration curve for the 1-meter spectrometer and E-photomultiplier detector. The plot shows the relative inverse spectral sensitivity over the range 220-500 nm. Associated error bars are shown.

Figure 2. Calibrated MUV-visible emission spectra of H_2 within the wavelength range 175-530 nm produced by electron impact at a) 14 eV, b) 19 eV, and c) 100 eV, measured at a spectral resolution of 1.7 nm (FWHM). Spectra are measured using an E-photomultiplier tube (E-PMT) at wavelengths above 220nm, and using an F-photomultiplier tube (F-PMT) at wavelengths below 220 run. The spectra were obtained at a gas temperature of 300 "K and a background gas pressure of 2.4x104 torr. Spectral feature numbers are identified. Band cross sections and spectroscopic assignments are given in Table 1.

References

Ajello, J. M., G.K. James, B.O. Franklin and D.E. Shemansky, Medium-Resolution Studies of Extreme Ultraviolet Emission from N_2 by Electron Impact: Vibrational Perturbations and Cross Sections of the $c_4'\,^1\Sigma_u^+$ and $b'\,^1\Sigma_u^+$ States, *Physical Review A*, *40,3524,* 1989.

Ajello, J.M. and D.E. Shemansky, Electron Excitation of the H_2 ($a\,^3\Sigma_g^+ \rightarrow b\,^3\Sigma_u^+$) Continuum in the Vacuum Ultraviolet, *The Astrophysical Journal, 407, 820,* 1993.

Ajello, J. M., *et al.,* Simple Ultraviolet Calibration Source with Reference Spectra and its use with the Galileo Orbiter Ultraviolet Spectrometer, *Applied Optics, 27,980,* 1988.

Anderson, R. J., J. Watson, Jr. and F.A. Sharpton, Electron Impact Excitation of the G $^1\Sigma_g^+$ State of H_2, *Journal of the Optical Society of America, 67,* 1641, 1977.

Crosswhite, H. M., The Hydrogen Molecule Wavelength Tables of Gerhard Heinrich Dieke, *Wiley-Interscience, New York, 1972.*

Day, R. L., R.J. Anderson and F.A. Sharpton, Electron Excitation of the Singlet-g States of H_2, *Journal of Chemical Physics, 71,3683,* 1979.

Dieke, G. H., The Molecular Spectrum of Hydrogen and its Isotopes, *Journal of Molecular Spectroscopy, 2, 494,* 1958.

James, G.K., J.M. Ajello, I. Kanik, B. Franklin and D.E. Shemansky, The Extreme Ultraviolet Emission Spectrum of CO Produced by Electron Impact at 20 and 200 eV, *Journal of Physics B: Atomic, Molecular, and Optical Physics, 25,* 1481, 1992.

Karolis, C. and E. Harting, Electron Impact Dissociation Cross Sections in Hydrogen and Deuterium, Leading to Balmer Alpha and Beta Emission, *Journal of Physics B: Atomic and Molecular Physics, 11,347, 1978.*

Pryor, W. R., J.M. Ajello, W.K. Tobiska, D.E. Shemansky, G.K. James, C.W. Herd, S. Stephens, R.A. West, I.F. Stewart, W.E. McClintock, C.A. Barth and K.E. Simmons, Galileo Ultraviolet Spectrometer Observations of Jupiter's Auroral Spectrum from 160-320 nm, *Journal of Geophysical Research (Planets),* this issue, 1998.

Ross, S.C. and Ch. Jungen, Multichannel Quantum-Defect Theory of Double-Minimum $^1\Sigma_g^+$ States in H,. I. Potential-Energy Curves, *Physical Review A, 49,4353,* 1994a,

Ross, S.C. and Ch. Jungen, Multichannel Quantum-Defect Theory of Double-Minimum $^1\Sigma_g^+$ States in H_2. II. Vibronic-Energy Levels, *Physical Review A, 49,4364,* 1994b.

Ross, S.C. and Ch. Jungen, Multichannel Quantum-Defect Theory of n=2 and 3 Gerade States in H_2: Rovibronic Energy Levels, *Physical Review A, 50,4618, 1994c.*

Senn, P. and K. Dressier, Spectroscopic Identification of Rovibronic Levels Lying Above the Potential Barrier of the $EF\,^1\Sigma_g^+$ Double-Minimum State of the H_2 Molecule, *Journal of Chemical Physics, 87,6908, 1987.*

Tsukiyama, K., J. Ishii and T. Kasuya, Fluorescence Lifetimes of $EF\,^1\Sigma_g^+$, $GK\,^1\Sigma_g^+$, $H\,^1\Sigma_g^+$, $I\,^1\Pi_g$ and $J\,^1\Delta_g$ States of H_2 Studied by Extreme Ultraviolet-Visible Double Resonance Excitation, *Journal of Chemical Physics, 97, 875,* 1992.

Vroom, D.A. and F.J. de Heer, Production of Excited Atoms by Impact of Fast Electrons on Molecular Hydrogen and Deuterium, *Journal of Chemical Physics, 50,580, 1969.*

Watson, J.,Jr., and R.J. Anderson, Excitation of the $E,F\,^1\Sigma_g^+$ States of H_2 by Electron Impact, *Journal of Chemical Physics*, *66,4025, 1977.*

Wolniewicz, L and K. Dressier, The *EF* and $GK\,^1\Sigma_g^+$ States of Hydrogen (Adiabatic Calculation of Vibronic States in H_2, HD, and D_2), *Journal of Molecular Spectroscopy, 67,416,* 1977.

Wolniewicz, L. and K. Dressier, Adiabatic Potential Curves and Nonadiabatic Coupling Functions for the First Five Excited $^1\Sigma_g^+$ States of the Hydrogen Molecule, *Journal of Chemical Physics,* 100,444, 1994.

Yu, S. and K. Dressier, Calculation of Rovibronic Structures in the Lowest Nine Excited $^1\Sigma_g^+ + {}^1\Pi_g + {}^1\Delta_g$ States of H_2, D_2, and T_2, *Journal of Chemical Physics, 101,7692,* 1994.

Figure 1

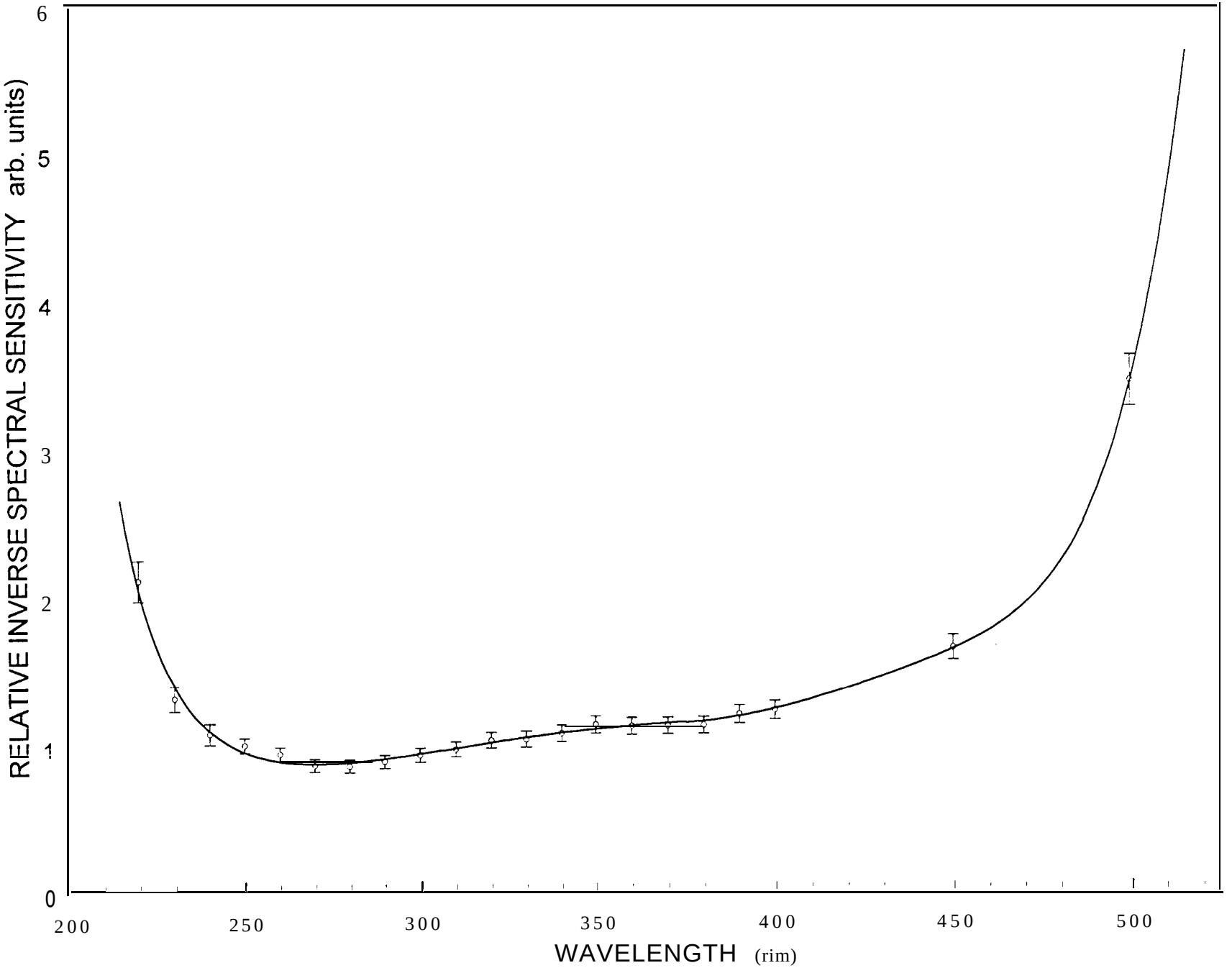
RELATIVE INVERSE SPECTRAL SENSITIVITY arb. units)
6
5
4
3
2
1
0
200
250
300
350
400
450
500
WAVELENGTH (rim)

Figure 2a

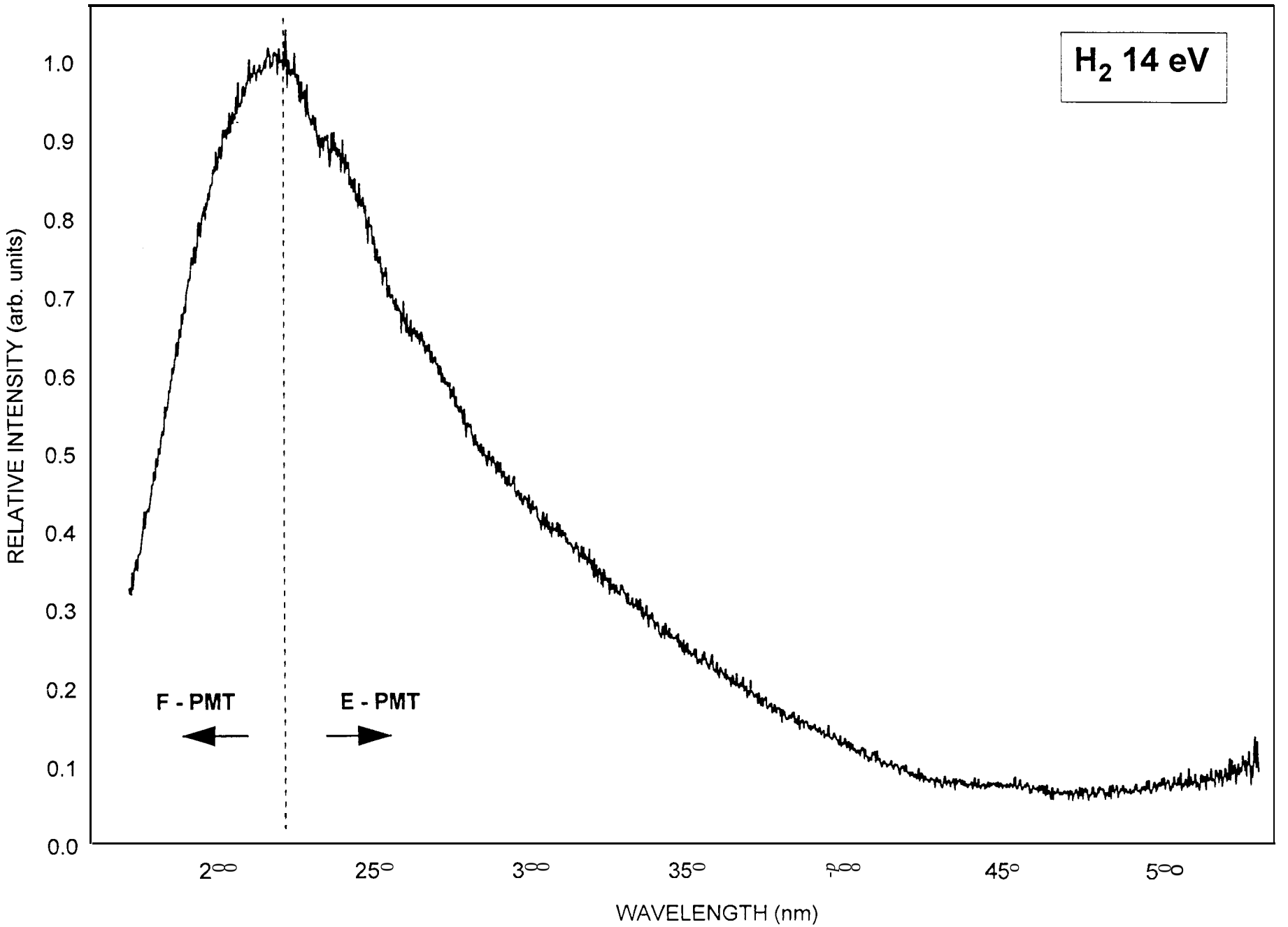
H_2 14 eV
RELATIVE INTENSITY (arb. units)
1.0
0.9
0.8
0.7
0.6
0.5
0.4
0.3
0.2
0.1
0.0
F - PMT
E - PMT
2∞
25°
3∞
35°
4∞
45°
5∞
WAVELENGTH (nm)

Figure 2b

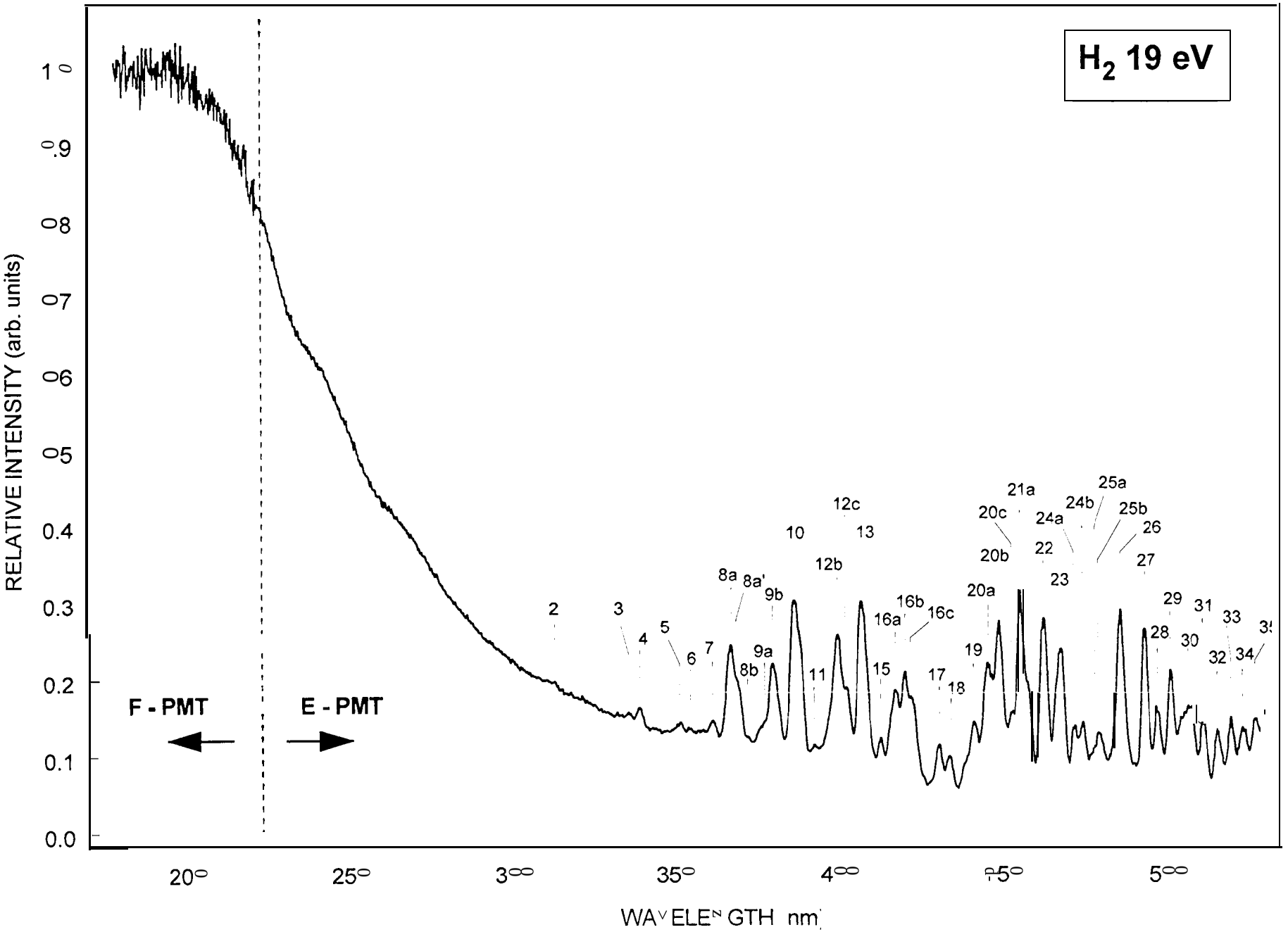
H2 19 eV
RELATIVE INTENSITY (arb. units)
1.0
0.9
0.8
0.7
0.6
0.5
0.4
0.3
0.2
0.1
0.0
F - PMT
E - PMT
2
3
4
5
6
7
8a
8a'
8b
9a
9b
10
11
12b
12c
13
15
16a
16b
16c
17
18
19
20a
20b
20c
21a
22
23
24a
24b
25a
25b
26
27
28
29
30
31
32
33
34
20
25
3
35
4
45
5
WAVELENGTH nm

Figure 2c

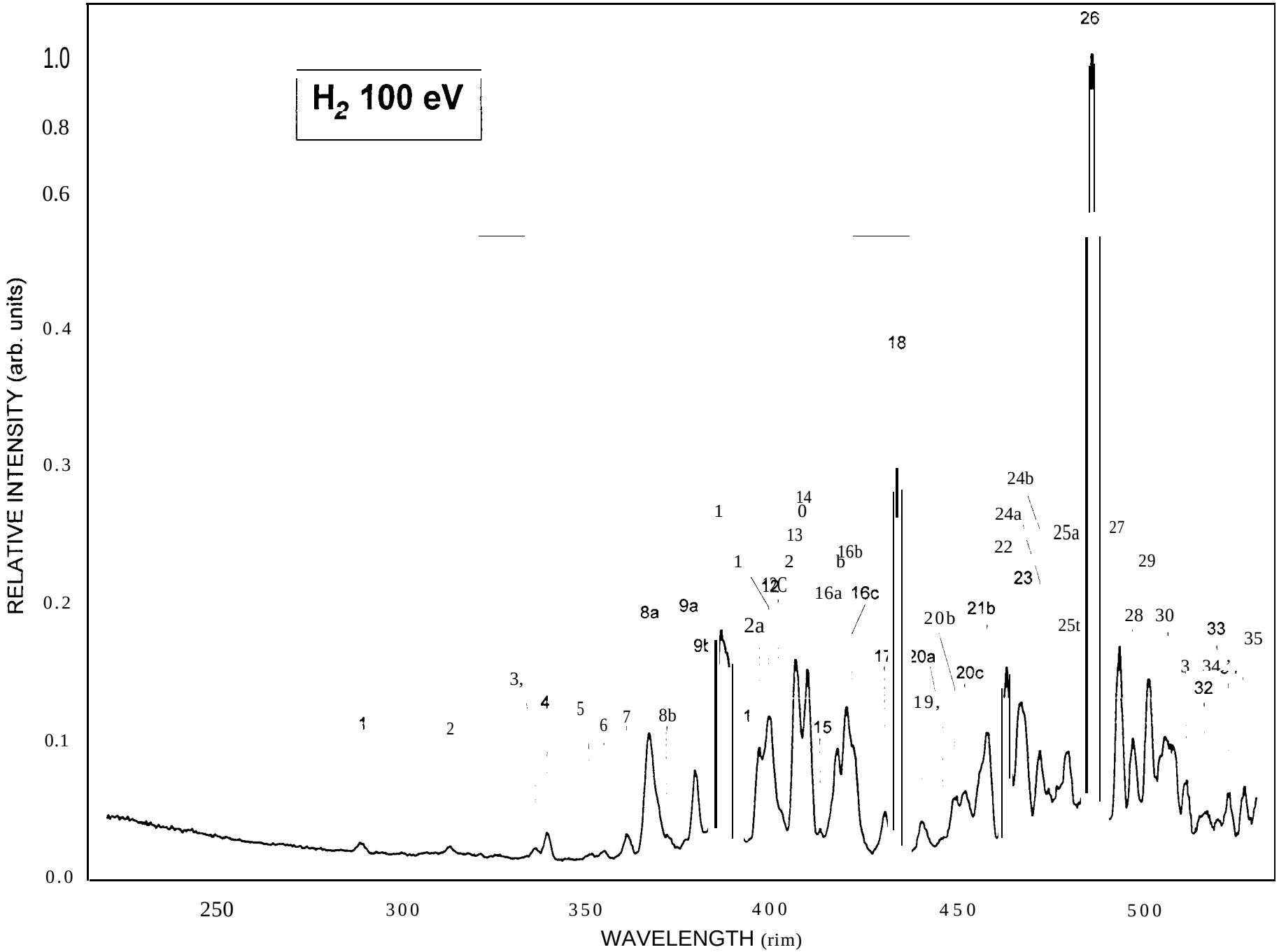
H2 100 eV
RELATIVE INTENSITY (arb. units)
1.0
0.8
0.6
0.4
0.3
0.2
0.1
0.0
250
300
350
400
450
500
WAVELENGTH (rim)
26
18
1
2
3,
4
5
6
7
8b
8a
9a
9t
2a
1
1
2
12C
16a
16c
16b
b
14
0
13
15
17
20a
19,
20b
20c
21b
24b
24a
22
23
25a
25t
27
29
28
30
33
35
32

Table 1

Feature Number	Integrated λ (rim)	Emission Cross Section (xl 0^{-20} cm*)		Observed Peak λ (rim)		Assignment
		19 eV	100 eV	19 eV	100 eV	
1	...	...		...	...	...
	286.5 -291.0		0.58		289.0	
2	310.4-315.1	4.58		312.9	313.0	...
	310.3 -315.0		0.52			
3	334.4 -337.6	2.54		336.1	336.3	.
	334.3 -337.3		0.32			
4	337.9-341.6	2.88		339.4	339.5	R $^1\Pi_g$ - B $^1\Sigma_u^+$ (1,0) Q1, Q2, Q3, Q4
	337.5 -341.5		0.56			
5	349.6 -353.4	2.63		351.6	351.0	*4e* $^3\Pi$ - 2C $^3\Pi$ *(3,0) R1,* R3
	349.0-352.3		0.27			
6	353.6-357.6	2.69		355.1	355.3	R $^1\Pi_g$ - B $^1\Sigma_u^+$ (1,1) Q1, Q2, Q3, Q4
	352.5 -356.8		0.38			4e $^3\Pi$ - *2c* $^3\Pi$ *(3,0)* P3
7	360.1 -363.9	2.63		361.9	361.8	G, K $^1\Sigma_g^+$ - B $^1\Sigma_u^+$ (3,0) RO, RI
	359.5 -363.3		0.54			I $^1\Pi_g$ - B $^1\Sigma_u^+$ (3,0) Q1, Q2, Q3, P2
						R $^1\Pi_g$ - B $^1\Sigma_u^+$ (2,3) Q 2
						S ^1A_g - B $^1\Sigma_u^+$ (0,0) Q3, P4

Feature Number	integrated λ (rim)	Emission Cross Section ($x10^{-20}$ cm')		Observed Peak λ (rim)			Assignment
		19 eV	100 eV	19 eV	100 eV		
8	364.1 -373.9 364.5 -374.3	8.08	3.28	a :367.6	a: 367.5	8a	H $^1\Sigma_g^+$ – B $^1\Sigma_u^+$(2,0) R1 T – B $^1\Sigma_u^+$(0,0) RO, R1 P $^1\Sigma_g^+$ - B $^1\Sigma_u^+$(0,0) R0, P1, R5
				a′: 369.1		8a'	P $^1\Sigma_g^+$ - B $^1\Sigma_u^+$(0,0) P2 T - B $^1\Sigma_u^+$(0,0) P1 J $^1\Delta_g$ - B $^1\Sigma_u^+$(3,1) Q2 G, K $^1\Sigma_g^+$ - B $^1\Sigma_u^+$(3,0) P6
				b :372.6	b :372.3	8b	R $^1\Pi_g$ - B $^1\Sigma_u^+$(1,2) Q2, Q3 *W* - B $^1\Sigma_u^+$(2,0) P1
9	374.4-383.4 375.0-382.5	6.98	1.89	a :377.6	a: 377.8	9a	I $^1\Pi_g$ - B $^1\Sigma_u^+$(3,1) Q7, RI *4c* $^3\Pi$ - 2a% (5,0) *Q3* *4c* ^{3}11 – *2a* $^3\Sigma$*(2,0) Q3* S $^1\Delta_g$ – B $^1\Sigma_u^+$(0,1) P5 J ^1A_g - B $^1\Sigma_u^+$(2,0) Q2
				b :380.1	b :380.0	9b	G, K $^1\Sigma_g^+$ - B $^1\Sigma_u^+$(3,1) R0, R1, R2 I $^1\Pi_g$ – B $^1\Sigma_u^+$(3,1) Q2, Q1, P2 i $^1\Pi_g$ - B $^1\Sigma_u^+$(2,0) R4 S $^1\Delta_g$ – B $^1\Sigma_u^+$(0,1) Q3, P4

Feature Number	Integrated λ (rim)	Emission Cross Section ($x10^{-20}$ cm')		Observed Peak λ (rim)		Assignment
		19 eV	100 eV	19 eV	100 eV	
10	383.6-390.9 382.8-391.0	7.26	5.51	386.9	387.5	Balmer H_8 (n = 8) H $^1\Sigma_g^+$ – B $^1\Sigma_u^+$ (2,1) R0 Z– B $^1\Sigma_u^+$ (2,0) RO, RI, R3 P $^1\Sigma_g^+$ – B $^1\Sigma_u^+$ (0,1) R1, R2, R3, R4 G, K $^1\Sigma_g^+$ - B $^1\Sigma_u^+$ (3,1) P6 G, K $^1\Sigma_g^+$ - B $^1\Sigma_u^+$ (2,0) R4, R5 *T* – B $^1\Sigma_u^+$ (0,1) R0 J $^1\Delta_g$ - B $^1\Sigma_u^+$ (3,2) Q2
11	391.4-394.4 391.3 -394.0	1.72	0.48	392.6	392.3	W– B $^1\Sigma_u^+$ (2,1) P2 P $^1\Sigma_g^+$ – B $^1\Sigma_u^+$ (0,1) P6

Feature Number	Integrated λ (nm)	Emission Cross Section ($x10^{-20}$ cm^2)		Observed Peak λ (nm)			Assignment
		19 eV	100 eV	19 eV	100 eV		
					a : 397.3	2a	Balmer H_ε (n = 7) I $^1\Pi_g$ – B $^1\Sigma_u^+$(3,2) R1, Q6 J $^1\Delta_g$ – B $^1\Sigma_u^+$(2,1) Q2 H $^1\Sigma_g^+$ – B $^1\Sigma_u^+$(1,0) R1
12	395.4-404.4 394.8-404.3	7.97	4 ≤	b 399.9	¤ : 399.8	12b	G, K $^1\Sigma_g^-$ – B $^1\Sigma_u^-$(3,2) R2 I $^1\Pi_g$ – B $^1\Sigma_u^+$(3,2) P2, P3, P4. R4 H $^1\Sigma_g^+$ – B $^1\Sigma_u^+$(1,0) P1 *5c* $^3\Pi$ – *2a* $^3\Sigma$ *(0,0) R2*
				c : 4⊃2.	c 402.3	12c	G, K $^1\Sigma_g^+$ – B $^1\Sigma_u^+$(3,2) P3 I $^1\Pi_g$ – B $^1\Sigma_u^+$(2,1) R2 H $^1\Sigma_g^+$ – B $^1\Sigma_u^+$(2,2) R4 *X* – B $^1\Sigma_u^+$(2,2) R2 *W* – B $^1\Sigma_u^+$(1,0) P1 *5c* $^3\Pi$ – *2a* $^3\Sigma$ *(0,0) Q1*

Feature Number	Integrated λ (rim)	Emission Cross Section ($x10^{20}$ cm')		Observed Peak λ (rim)		Assignment
		19 eV	100 eV	19 eV	100 eV	
13	404.6-411.1	6.37		407.1	406.8	G, K $^1\Sigma_g^+$ - B $^1\Sigma_u^+$ (2,1) R0, R1, R2, R3 4e $^3\Pi$ – 2C ^{3}11 (1, O) P4, Q4
	404.8-408.3		2.75			I $^1\Pi_g$ - B $^1\Sigma_u^+$ (2,1) Q1, **Q2** J $^1\Delta_g$ - B $^1\Sigma_u^+$ (1,0) Q4 p $^1\Sigma_g^+$ – B $^1\Sigma_u^+$ (0,2) R1, R2, R3, R4 *4f* $^3\Delta$ - *2c* $^3\Pi$ **(3,2)** *Q3*
14	408.5 -412.0		2.65		410.0	Balmer H_δ (n = 6) J $^1\Delta_g$ - B $^1\Sigma_u^+$ (1,0) Q2
15	411.6-414.1	1.47		413.1	413.3	*W* – B $^1\Sigma_u^+$ (2,2) P2 I $^1\Pi_g$ - B $^1\Sigma_u^+$ (1,0) Q8, R2
	412.3 -414.3		0.43			U - B $^1\Sigma_u^+$ (1,0) P2

Feature Number	Integrated λ (rim)	Emission Cross Section ($\times 10^{-20}$ cm^2) 19 eV	100 eV	Observed Peak λ (rim) 19 eV	100 eV		Assignment
16	414.4-426.9	8.81		a : 417.6	a : 418.0	16a	I $^1\Pi_g$ - B $^1\Sigma_u^+$ (1,0) P3, P4, Q1, Q2, Q3
							I $^1\Pi_g$ – B $^1\Sigma_u$ (3,3) Q5
							H $^1\Sigma_g^+$ - B $^1\Sigma_u^+$ (1,1) R2
	414.5 -427.0		5.43	b :420.6	b :420.5	16b	G, K $^1\Sigma_g^+$ – B $^1\Sigma_u^+$ (3,3) R0, R1, R2
							G, K $^1\Sigma_g$ - B $^1\Sigma_u^+$ (1,0) R2
							H $^1\Sigma_g^+$ - B $^1\Sigma_u^+$ (1,1) R0
							W – B $^1\Sigma_u^+$ (1,1) R2, R3
							Z- B $^1\Sigma_u^+$ (1,0) R0, R1
				C :422.1	C :422.0	16c	*4d* $^3\Pi$ – 2c $^3\Pi$ *(3,2) P3*
							H $^1\Sigma_g^+$ – B $^1\Sigma_u^+$ (1,1) P1
							G, K $^1\Sigma_g^+$ - B $^1\Sigma_u^+$ (1,0) P2
17	426.9-432.4	2.35		430.9	430.5		X- B $^1\Sigma_u^+$ (0,0) RO, RI, R2, R3
							4c $^3\Pi$ – *2a* $^3\Sigma$ *(4,3) Q1*
	427.3 -431.8		0,90				*T* – B $^1\Sigma_u^+$ (0,3) P3
							Z- B $^1\Sigma_u$ (2,2) R0, R1
18	432.6-436.4	1.57		434.4	434.0		Balmer H_γ (n = 5)
	432.0-436.8		4.34				Y- B $^1\Sigma_u^+$ (1,0) P1, R2
							X- B $^1\Sigma_u^+$ (0,0) P3

Feature Number	Integrated λ (rim)	Emission Cross Section ($\times 10^{-20}$ cm')		Observed Peak λ (rim)			Assignment
		19 eV	100 eV	19 eV	100 eV		
19	436.6-442.9 437.0-443.8	3.29	1.13	441.4	440.5		H $^1\Sigma_g^+$ - B $^1\Sigma_u^+$ (0,0) P1, P2, P4 4c $^3\Pi$ – 2a $^3\Sigma$ (5,4) Q4 4e $^3\Pi$ – *2c* $^3\Pi$ (0,0) Q2, Q3, *RI, R2* *4e* $^3\Pi$ – *2c* $^3\Sigma_u^+$ *(1,1) R2* J $^1\Delta_g$ - B $^1\Sigma_u^+$ (0,0) R3 *4f* $^3\Delta$ - *2c* $^3\Pi$ *(1,1)* Q3 4f ^{3}A – *2c* $^3\Pi$ *(2,2)* R2
20	443.1 -453.6 444.0-454.0	9.57	2.86	a :445.9 b :449.1 C :452.9	a :446.0 b :449.3 c :452.0	20a 20b 20C	*4d* $^3\Sigma$ – **2c** $^3\Pi$ *(0,0)* R2 4c $^3\Pi$ - *2a% (0,0) R2* J ^1A_g - B $^1\Sigma_u^+$ (0,0) P6, Q4 *4b* $^3\Sigma$ – *2a* $^3\Sigma$ *(1,0)* P3 *4f* $^3\Delta$ - 2c $^3\Pi$ (2,2) Q2 4c $^3\Pi$ – *2a* $^3\Sigma$ *(0,0) QI,* **Q2** I $^1\Pi_g$ – B $^1\Sigma_u^+$ (0,0) Q9, R3 X- B $^1\Sigma_u^+$ (2,4) P3 *2u – 2a* $^3\Sigma$ **(2, O) P2** *4f* $^3\Delta$ – **2c** $^3\Pi$ *(2,2)* P3 Z- B $^1\Sigma_u^+$ (1,1) P2 *W* – B $^1\Sigma_u^+$ (1,2) P6 I $^1\Pi_g$ – B $^1\Sigma_u^+$ (2,3) P2, P4, Q3 *4c* $^3\Pi$ – *2a* $^3\Sigma$ *(0,0) P2* *4e* $^3\Pi$ - *2c* $^3\Pi$ *(2,2) P5*

Feature Number	Integrated λ (rim)	Emission Cross Section ($\times 10^{-20}$ cm') 19 eV	100 eV	Observed Peak λ (rim) 19 eV	100 eV		Assignment
21	453.9-459.9 454.3 -460.0	6.05	2.92	a : 455.6		21a	$4c\ ^3\Pi$ - *2a* $^3\Sigma$ *(1, 1) Q1,* Q2 G, K $^1\Sigma_g^+$ - B $^1\Sigma_u^+$ (1,1) P9 Z- B $^1\Sigma_u^+$ (2,3) R2 *4d* $^3\Sigma$ - *2c* ^{3}*11 (1,1)* Q4 *W* – B $^1\Sigma_u^+$ (2,4) R4 *5c* $^3\Pi$ – *2a* $^3\Sigma$ (2,3) Q.2
					b : 458.0	21b	I $^1\Pi_g$ - B $^1\Sigma_u^+$ (0,0) Q1, Q2, Q3, P3 G, K $^1\Sigma_g^+$ – B $^1\Sigma_u^+$ (0,0) R8 4e $^3\Pi$ - *2c* $^3\Pi$ *(3,3) R1*
22	460.1 -464.9 *460.3 -464.8*	4.53	*2.66*	462.6	463.3		G, K $^1\Sigma_g^+$ – B $^1\Sigma_u^+$ (0,0) RO, R1, R2, R4, R5 *4c* $^3\Pi$ - 2a $^3\Sigma$ *(1,1) P5* *4c* $^3\Pi$ – *2a* $^3\Sigma$ *(2,2) Q3* *U*- B $^1\Sigma_u^+$ (1,2) P2 Y- B $^1\Sigma_u^+$ (2,4) PI
23	465. i-469.9 465.0-469.8	4.27	3.30	467.9	467.3		I $^1\Pi_g$ - **B** $^1\Sigma_u^+$ (1,2) Q3, Q4 G, K $^1\Sigma_g^+$ - B $^1\Sigma_u^+$ (3,5) R0, R1, R2 G, K $^1\Sigma_g$ - B $^1\Sigma_u^+$ (0,0) P3 H $^1\Sigma_g^+$ - B $^1\Sigma_u^+$ (0,1) P2, P3, P4 Z- B $^1\Sigma_u^+$ (0,0) P1, R3 $4c\ ^3\Pi$ - *2a* $^3\Sigma$ (3,3) *Q1*

Feature Number	Integrated λ (nm)	Emission Cross Section ($x10^{-20}$ cm^2) 19 eV	Emission Cross Section ($x10^{-20}$ cm^2) 100 eV	Observed Peak λ (nm) 19 eV	Observed Peak λ (nm) 100 eV		Assignment
24	470.4-475.9 470.0-475.0	3.4	2. 4	a : 471.9	a : 472.0	24a	G, K $^1\Sigma_g^+$ – B $^1\Sigma_u^+$ (1,2) R2, R5 G, K $^1\Sigma_g^+$ – B $^1\Sigma_u^+$ (0,0) P6, P10 *4e* $^3\Pi$ – *2c* $^3\Pi$ *(2,0) Q6* *V* – B $^1\Sigma_u^+$ (0,0) R0
				b : 474.4	b : 474.3	24b	*4c* $^3\Pi$ – *2a* $^3\Sigma$ *(4,4) Q1* *Z* – B $^1\Sigma_u^+$ (1,2) R0, R1, R2 J $^1\Delta_g$ – B $^1\Sigma_u^+$ (1,3) Q6 *W* – B $^1\Sigma_u^+$ (1,3) R0
25	476.1-481.6 475.3-481.8	3.0≤	3 °8	a : 478.1	a : 476.5	25a	P $^1\Sigma_g^+$ – B $^1\Sigma_u^+$ (0,5) R4 *3e* $^3\Pi$ – *2c* $^3\Pi$ *(2,0) P3* *W* – B $^1\Sigma_u^+$ (1,3) P2, P3. P4 I $^1\Pi_g$ – B $^1\Sigma_u^+$ (2,4) P4
				b : 479.4	b : 479.5	25b	G, K $^1\Sigma_g^+$ – B $^1\Sigma_u^+$ (2,4) R0, R1, R2, R3 I $^1\Pi_g$ – B $^1\Sigma_u^+$ (2,4) P2, Q3 *4d* $^3\Sigma$ – *2c* $^3\Pi$ *(2,0) Q1*
26	482.9-489.4 483.5-489.3	5. 7	15.30	486.1	48≤ 1		Balmer H_β (n = 4) I $^1\Pi_g$ – B $^1\Sigma_u^+$ (0,1) P4, Q4 *4f* $^3\Delta$ – *2c* $^3\Pi$ *(0,1) Q2* *3e* $^3\Pi$ – *2c* $^3\Pi$ *(3,1) P2* *4b* $^3\Sigma$ – *2a* $^3\Sigma$ *(0,0) R0* *W* – B $^1\Sigma_u^+$ (2,5) P2

Feature Number	Integrated λ (rim)	Emission Cross Section ($x10^{-20}$ cm^2)		Observed Peak λ (rim)		Assignment
		19 eV	100 eV	19 eV	100 eV	
27	491.1 -495.4 491.5 -495.0	3.77	2.75	493.4	493.5	G, K $^1\Sigma_g^+$ – B $^1\Sigma_u^+$ (0,1) R1, R2, R3, P1 G, K $^1\Sigma_g^+$ – B $^1\Sigma_u^+$ (3,6) R0 I $^1\Pi_g$ – B $^1\Sigma_u^+$ (3,6) Q1 J $^1\Delta_g$ – B $^1\Sigma_u^+$ (0,2) R4 *Y* – B $^1\Sigma_u^+$ (2,5) P4 *4e* $^3\Pi$ - 2c $^3\Pi$ (1,2) *R 5* *3d* $^3\Sigma$ – *2c* $^3\Pi$ *(3, 1) R2*
28	495.6 -498.9 495.3 -499.0	2.23	1.99	497.4	497.0	I $^1\Pi_g$ - B $^1\Sigma_u^+$ (1,3) Q2, Q3, P4 Z - B $^1\Sigma_u$ (0,1) R2 H $^1\Sigma_g^+$ – B $^1\Sigma_u^+$ (0,2) P2
29	499,4 -502.9 499.3 -503.0	2.85	2.69	501.1	501.3	G, K $^1\Sigma_g^+$ - B $^1\Sigma_u^+$ (1,3) R1, R2, R4, P1 H $^1\Sigma_g^+$ - B $^1\Sigma_u^+$ (1,4) P1, P4 J $^1\Delta_g$ – B $^1\Sigma_u^+$ (3,7) Q2 *W* – B $^1\Sigma_u^+$ (1,4) R2 4g - *2a* $^3\Sigma$ (1,2) *P5* *4d* $^3\Sigma$ - *2c* ^{3}**11 (1,2)** Q2
30	503.1 -509.4 503.3 -509.5	4.51	3.78	506.6	506.3	*W* – B $^1\Sigma_u^+$ (1,4) P3, P4 I $^1\Pi_g$ – B $^1\Sigma_u^+$ (2,5) Q4 J $^1\Delta_g$ – B $^1\Sigma_u^+$ (1,4) Q5 Z - B $^1\Sigma_u^+$ (1,3) P2

Feature Number	Integrated λ (rim)	Emission Cross Section ($\times 10^{-20}$ cm²) 19 eV	100 eV	Observed Peak λ (rim) 19 eV	100 eV	Assignment
31	509.6-512.9 509.8 -512.5	1.96	1.15	511.1	511.3	4e $^3\Pi$ - *2c* $^3\Pi$ (3, 4) *P2* Z– B $^1\Sigma_u^+$ (2,5) R1, R2 **3f** $^3\Delta$ - *2c* $^3\Pi$ *(2, 1) R2* *4c* $^3\Pi$ - *2a* $^3\Sigma$ *(1,2) Q1*
32	513.4 -517.4 514.0-518.3	2.18	1.23	515.4	516.0	*W* – B $^1\Sigma_u^+$ (2,6) P3 *4c* $^3\Pi$ - *2a* $^3\Sigma$ *(2,3)* Q], *Q2, Q3* *3f* $^3\Delta$ - *2c* $^3\Pi$ (2, 1) *Q2* *X* – B $^1\Sigma_u^+$ (0,3) R2
33	517.9-521.4 518.5 -520.5	2.11	0.57	519.9	519.5	I $^1\Pi_g$ - **B** $^1\Sigma_u^+$ (0,2) Ql, Q2, Q3, P2 I $^1\Pi_g$ - B $^1\Sigma_u^+$ (3,7) RO, Q4 *3a* $^3\Sigma$ - *2c* $^3\Pi$ *(1,0)* Q4 Y- B $^1\Sigma_u^+$ (1,3) R0 Y- B $^1\Sigma_u^+$ (2,6) P2 4C $^3\Pi$ - *2a* $^3\Sigma$ *(3,4) Q1* *3f* $^3\Delta$ - *2c* ^{3}11 *(3,2) RI*
34	521.6 -525.1 520.8 -524.0	2.17	1.08	523.4	522.5	G, K $^1\Sigma_g^+$ - B $^1\Sigma_u^+$ (3,7) R0, R1, R2 I $^1\Pi_g$ – B $^1\Sigma_u^+$ (1,4) R2 I $^1\Pi_g$ - B $^1\Sigma_u^+$ (3,7) Q1, P4 Y- B $^1\Sigma_u^+$ (1,3) P2 *4b* $^3\Sigma$ - *2a* $^3\Sigma$ *(6,* 1) *P2*

Feature Number	Integrated λ (rim) .	Emission Cross Section ($x10^{20}$ cm')		Observed Peak λ (rim)		Assignment
		19 **eV**	100 **eV**	19 **eV**	100 **eV**	
35	525.4-528.6 524.3 -528.3	2.22	1.29	527.1	526.5	**G,** K $^1\Sigma_g^+$ – B $^1\Sigma_u^+$(0,2) **RO,** R1, R2, R3 **I** $^1\Pi_g$ - **B** $^1\Sigma_u^+$(1,4) **RO, Q4** **R** $^1\Pi_g$ – **B** $^{+1}\Sigma_u$ (0,7) R0 **3*** $^3\Sigma$ - *2c* $^3\Pi$ *(1,0)* **P 4** 3c $^3\Pi$ - *2a* $^3\Sigma$ *(1,0) R1* *3b* $^3\Sigma$ - *2a* $^3\Sigma$ (4,0) *PI*